Canadian Geotechnical Journal, Vol. 50, No. 12, pp. 1260-1272, 2013

On the "elastic stiffness" in a high-cycle accumulation model - continued investigations

T. Wichtmann[i)], A. Niemunis[ii)], Th. Triantafyllidis[iii)]

Abstract: The high-cycle accumulation (HCA) model proposed by the authors can be used to predict permanent deformations or stress relaxation due to a large number (e.g. several millions) of load cycles with relative small strain amplitudes ($< 10^{-3}$). The predicted stress relaxation depends on the isotropic "elastic stiffness" E used in the HCA model. In order to calibrate the bulk modulus K, the rate of pore pressure accumulation obtained from an undrained cyclic test and the rate of volumetric strain accumulation measured in a drained cyclic test are compared. Poisson's ratio ν can be determined from the shape of the stress relaxation path measured in an undrained test with anisotropic consolidation stresses and strain cycles. Unfortunately, the calibration of K shown for a medium coarse sand in the previous paper [20] was affected by membrane penetration effects. Consequently, all further studies have been performed on a fine sand for which membrane penetration is negligible. The present paper reports on the new results. The strong pressure-dependence of K and its independence of amplitude found in the previous study could be confirmed by the new tests. In addition, the new experimental results reveal a density-dependence of K, while the bulk modulus is rather independent of stress ratio. Furthermore, for the first time Poisson's ratio ν used in the HCA model has been calibrated based on tests performed with different amplitudes, densities and initial stresses.

Keywords: High-cycle accumulation model; elastic stiffness; bulk modulus; Poisson's ratio; cyclic tests; fine sand

1 Introduction

High-cycle accumulation (HCA) models can be used for the prediction of permanent deformations or stress relaxation in non-cohesive soils caused by a large number ($N > 10^3$) of cycles with relative small strain amplitudes ($\varepsilon^{\mathrm{ampl}} < 10^{-3}$) (so-called high-cyclic loading). Typical applications involve several thousands up to millions of load cycles. Examples are offshore wind power plants, where the cyclic loading is caused by wind and waves, or machine foundations. Other practical problems with high-cyclic loading are foundations subjected to traffic (e.g. railways of high-speed trains or magnetic levitation trains) and tanks, silos and watergates, where the cyclic loading is due to the changing height of the filling. Several HCA models have been proposed in the literature (e.g. [1, 2, 6, 8, 10, 12]). Deficits of some of these models (e.g. lack of generality, missing influencing parameters, 1D formulation) have been discussed in [16].

The HCA model proposed by Niemunis et al. [10] is used in the framework of a special finite element calculation strategy. It is illustrated for a shallow foundation in Fig. 1. Only a few cycles are calculated with a conventional constitutive model, e.g. an elastoplastic multi-surface or a hypoplastic model. Larger packages of cycles between are treated with the HCA model. This model takes an increment of the number of cycles ΔN as input and predicts the resulting permanent strain directly, without tracing the oscillating strain path during the individual cycles. During the calculation with the HCA model the external load is kept constant on its average value (Fig. 1). Therefore, the accumulation of permanent strain due to cyclic loading is treated similar to a creep deformation in viscoplastic models.

[i)] Researcher, Institute of Soil Mechanics and Rock Mechanics (IBF), Karlsruhe Institute of Technology (KIT), Germany (corresponding author). Email: torsten.wichtmann@kit.edu

[ii)] Researcher, IBF, KIT, Germany

[iii)] Professor and Director of the IBF, KIT, Germany

The conventional calculation of the first two cycles (Fig. 1) is necessary in order to determine the spatial field of the strain amplitude which is an important input parameter of the HCA model. The deformations during the first cycle may be significantly larger than those in the subsequent cycles. Therefore, the strain amplitude is determined from the second cycle which is more representative for the elastic portion of deformation during the subsequent cycles. The strain amplitude is evaluated from the strain path recorded in each integration point [10]. During the calculation with the HCA model, the strain amplitude is assumed constant. However, the real spatial field of the strain amplitude may change due to compaction or re-distribution of stress. Therefore, in order to update the field of the strain amplitude, the calculation with the HCA model should be interrupted after definite numbers of cycles (e.g. at $N =$ 10, 100, 1000, etc.) and a *control cycle* should be calculated conventionally (Fig. 1).

Although sophisticated elastoplastic or hypoplastic models have been developed with focus to cyclic loading (see e.g. the review of elastoplastic models given by Zhang & Wang [23] and their bounding surface model), the calculation strategy shown in Fig. 1 is more suitable for a large number of cycles than the conventional one since the number of calculated increments and thus both the numerical error and the calculation effort (especially in the case of 3D prolems) are much smaller.

The basic assumption of the HCA model proposed by Niemunis et al. [10] is that the strain path and the stress path resulting from a high-cyclic loading can be decomposed into an oscillating part and a trend. The HCA model takes the oscillating part (strain amplitude $\varepsilon^{\mathrm{ampl}}$) as input and predicts the trend. The "elastic stiffness" E discussed in this paper is used in the basic constitutive equation of the HCA model

$$\dot{\boldsymbol{\sigma}}^{\mathrm{av}} = \mathsf{E} : (\dot{\boldsymbol{\varepsilon}}^{\mathrm{av}} - \dot{\boldsymbol{\varepsilon}}^{\mathrm{acc}} - \dot{\boldsymbol{\varepsilon}}^{\mathrm{pl}}) \tag{1}$$

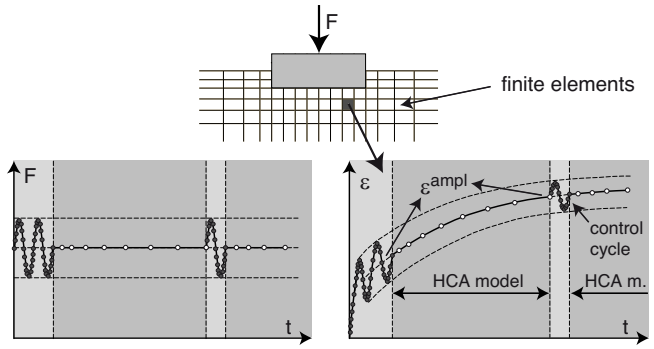

Fig. 1: *Strategy in FE calculations with the HCA model*

In the context of HCA models the dot over a symbol means the derivative with respect to the number of cycles N, i.e. $\dot{\sqcup} = \partial \sqcup / \partial N$. The "elastic stiffness" E interrelates the rate of effective Cauchy stress $\dot{\boldsymbol{\sigma}}^{\mathrm{av}}$ and the rate of strain $\dot{\boldsymbol{\varepsilon}}^{\mathrm{av}}$. The index $\sqcup^{\mathrm{av}}$ means the average value of a variable during a cycle. The accumulation rate $\dot{\boldsymbol{\varepsilon}}^{\mathrm{acc}} = \dot{\varepsilon}^{\mathrm{acc}}\mathbf{m}$ is calculated as the product of the *intensity* of accumulation $\dot{\varepsilon}^{\mathrm{acc}}$ and the *direction* of accumulation $\mathbf{m}$ (flow rule). The intensity $\dot{\varepsilon}^{\mathrm{acc}}$ depends on various factors [10]:

$$\dot{\varepsilon}^{\mathrm{acc}} \;=\; f_{\mathrm{ampl}}\; \dot{f}_N\; f_e\; f_p\; f_Y\; f_\pi \tag{2}$$

The six scalar functions consider the influences of strain amplitude (f_{ampl}), cyclic preloading ($\dot{f}_N$), average void ratio (f_e), average mean pressure (f_p), average stress ratio (f_Y) and changes in polarization (f_π). The multiplicative approach for $\dot{\varepsilon}^{\mathrm{acc}}$ was chosen heuristically and then to some extent confirmed experimentally [16–18]. The rate of accumulation depends strongly on several subtle properties of the soil like number of grain contacts, distribution of grain contact normals, arrangement of grains, fluctuation of stress, etc., i.e. $\dot{\varepsilon}^{\mathrm{acc}}$ cannot be expressed by the customary state variables (stress and void ratio) alone. Additional state variables (g^A, $\boldsymbol{\pi}$, see [10] or [20] for details) describing the cyclic loading history have been introduced into the HCA model phenomenologically, i.e. the relation to fabric is not investigated. They affect the rate of strain accumulation via $\dot{f}_N$ and f_π. The plastic strain rate $\dot{\boldsymbol{\varepsilon}}^{\mathrm{pl}}$ in Eq. (1) keeps the stress path within the Matsuoka-Nakai yield surface.

A simple isotropic stiffness $\mathsf{E} = K\mathbf{1}\otimes\mathbf{1} + 2G(\mathsf{I} - \frac{1}{3}\mathbf{1}\otimes\mathbf{1})$ with bulk modulus $K = E/[3(1-2\nu)]$, shear modulus $G = E/[2(1+\nu)]$, Young's modulus E, Poisson's ratio ν and two identity tensors $\mathbf{1}$ and I has been used in the HCA model so far. Two elastic constants (e.g. K and ν) need thus to be calibrated. Note that E need not be hyperelastic contrary to conventional models for cyclic loading, since the stress or strain path during the individual cycles is not calculated incrementally. The HCA model predicts the accumulation trends only and thus cannot contradict the second law of thermodynamics converting heat into work within a single cycle.

According to classical elasticity, the Young's modulus of a contact of two spheres obeys $E \sim p^{1/3}$ wherein p is pressure [5]. The stress-dependence $E \sim p^{1/2}$ derived for a contact of two cones [3] is more realistic for granular materials. Numerous empirical formulas have been proposed in the literature for the small-strain stiffness of sand. Formulations of type $E = A\, F(e)\, p^n$ originating from Hardin and Richart [4] are wide-spread. The constants A and n depend on the grain size distribution curve and grain characteristics. Typical values for the exponent n range from 0.4 for poorly graded sands to 0.6 for well-graded materials [21]. Hyperbolic or exponential functions are usually applied for the void ratio function $F(e)$. Theoretically the Poisson's ratio ν must lie between -1 and 0.5 but negative values of ν are highly improbable for physical reasons [7]. Typical values for sand derived from wave velocity measurements lie in the range $0.2 \le \nu \le 0.4$ [22]. However, all these considerations based on classical elasticity or experiments related to small-strain stiffness may not apply to the stiffness E used in a HCA model, since it does not interrelate stress and strain rates but accumulation trends.

In conventional constitutive models the tangent stiffness $\mathsf{E} = \partial\dot{\boldsymbol{\sigma}}/\partial\dot{\boldsymbol{\varepsilon}}$ can be determined experimentally from a small (monotonic) unloading. Under cyclic loading Eq. (1) returns creep $\dot{\boldsymbol{\varepsilon}}^{\mathrm{av}} = \dot{\boldsymbol{\varepsilon}}^{\mathrm{acc}}$ at $\dot{\boldsymbol{\sigma}}^{\mathrm{av}} = \mathbf{0}$ or relaxation $\dot{\boldsymbol{\sigma}}^{\mathrm{av}} = -\mathsf{E}\dot{\boldsymbol{\varepsilon}}^{\mathrm{acc}}$ at $\dot{\boldsymbol{\varepsilon}}^{\mathrm{av}} = \mathbf{0}$, so E interrelates creep and relaxation. Hence, the "elastic stiffness" E of a HCA model has to be determined from cyclic tests.

The bulk modulus K can be obtained from the relation [20]

$$K \;=\; -\frac{\dot{p}^{\mathrm{av}}}{\dot{\varepsilon}_v^{\mathrm{acc}}} \;=\; \frac{\dot{u}^{\mathrm{acc}}}{\dot{\varepsilon}_v^{\mathrm{acc}}} \tag{3}$$

with the rate of isotropic stress relaxation $\dot{p}^{\mathrm{av}}$ or pore pressure accumulation $\dot{u}^{\mathrm{acc}}$ obtained from an undrained cyclic test and the rate of volumetric strain accumulation $\dot{\varepsilon}_v^{\mathrm{acc}}$ measured in a drained cyclic test. Both, the drained and the undrained test should be performed with similar (possibly identical) initial densities, consolidation stresses and stress amplitudes.

Poisson's ratio ν can be quantified from the shape of the average effective stress path in the p-q plane, measured in a strain-controlled undrained cyclic test with anisotropic initial stresses. In that case, the ratio of deviatoric ($\dot{q}^{\mathrm{av}}$) and isotropic ($\dot{p}^{\mathrm{av}}$) stress relaxation predicted by the HCA model depends on ν ([20], see Figure 2):

$$\frac{\dot{q}^{\mathrm{av}}}{\dot{p}^{\mathrm{av}}} \;=\; \frac{9(1-2\nu)}{2(1+\nu)}\;\frac{2\eta^{\mathrm{av}}}{M^2 - (\eta^{\mathrm{av}})^2} \tag{4}$$

with average stress ratio $\eta^{\mathrm{av}} = q^{\mathrm{av}}/p^{\mathrm{av}}$ and

$$M \;=\; \frac{6\sin\varphi_c}{3-\sin\varphi_c}\cdot\begin{cases} 1 & \text{for } \eta^{\mathrm{av}} \ge 0 \\ 1+\eta^{\mathrm{av}}/3 & \text{for } \eta^{\mathrm{av}} < 0 \end{cases} \tag{5}$$

φ_c is the critical friction angle.

In [20] the calibration of K has been demonstrated for a medium coarse sand (mean grain size $d_{50} = 0.55$ mm). Unfortunately, the undrained cyclic tests performed on this sand were affected by membrane penetration effects. Although a correction has been applied in the evaluation of K, some uncertainty remained. Furthermore, only data for medium dense samples have been presented in [20]. The influence of density and average stress ratio on K has not been inspected in that earlier study. Stress relaxation experiments from which Poisson's ratio ν can be quantified were also not available at the time of the publication of [20].

The objective of this paper is the presentation of the experimental results that have been collected after completion of the study documented in [20]. In order to minimize membrane penetration effects all further tests have been performed on a fine sand with mean grain size $d_{50} = 0.14$ mm and uniformity coefficient $C_u = d_{60}/d_{10} = 1.5$. The

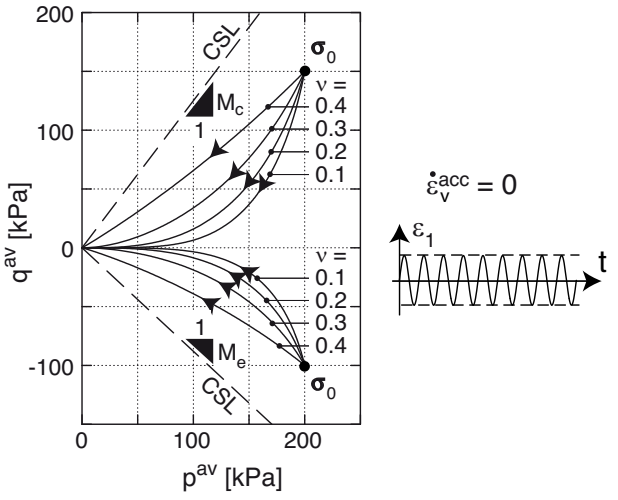

Fig. 2: *Average stress paths predicted by the HCA model for various ν-values*

grain shape is subangular and the minimum and maximum void ratios are $e_{\min} = 0.677$ and $e_{\max} = 1.054$. The specific gravity has been determined as $\varrho_s = 2.65$ g/cm^3. Due to the small grain sizes, membrane penetration effects are negligible for this sand. The dependence of bulk modulus K on pressure, amplitude, density and stress anisotropy has been inspected based on stress-controlled drained and undrained cyclic tests performed on the fine sand. Furthermore, strain-controlled tests with different amplitudes, densities and initial stresses have been conducted in order to calibrate Poisson's ratio ν.

2 Experimental study on bulk modulus K

All tests within the present experimental study were performed on triaxial specimens with diameter $d = 10$ cm and height $h = 10$ cm. The specimens were prepared by air pluviation and tested under water-saturated conditions. A back pressure of 500 kPa was used in most tests (in some tests 200 kPa was applied) in order to guarantee a high degree of saturation, i.e. a B-value larger than 0.99. The stress cycles were applied with a load press driven by a servomotor, using low displacement rates ≤ 0.05 mm/min.

2.1 Pressure- and amplitude-dependence

13 pairs of drained and undrained stress-controlled cyclic triaxial tests were performed in order to study the pressure- and amplitude-dependence of bulk modulus K. All samples were prepared with medium density $I_{D0} = (e_{\max} - e)/(e_{\max} - e_{\min}) = 0.51$ - 0.68 and consolidated under isotropic stresses. Five different initial pressures $p_0 = 50$, 100, 200, 300 and 500 kPa were applied. With the exception of $p_0 = 500$ kPa, for each initial pressure three different amplitude-pressure ratios $\zeta = q^{\text{ampl}}/p_0 = 0.2$, 0.25 and 0.3 were tested. A single amplitude ($\zeta = 0.25$) was applied at $p_0 = 500$ kPa. For each combination of initial pressure and amplitude, one sample was tested under drained conditions while another one was tested undrained. In the drained tests the initial and average pressures are identical, i.e. $p_0 = p^{\text{av}}$.

The HCA model describes the trends of stress and strain during the *regular* cycles only. The first *irregular* cycle, which may generate considerably larger residual strains or stress relaxation, is calculated with a conventional constitutive model (Fig. 1). For the calibration of K, the regular cycles in both, the drained and the corresponding undrained test should start from the same effective stress. For that purpose, the first irregular cycle was applied drained in all 26 tests, i.e. the average effective stress did not change during the first cycle. In the "undrained" tests the drainage was closed after the irregular cycle. The data from the first irregular cycle is not included in the following evaluation of K, i.e. $N = 1$ refers to the end of the first regular cycle.

The results of a typical undrained cyclic test are presented in Figure 3. Figure 3a shows the accumulation of pore water pressure u and the accompanying decrease of the lateral effective stress $\sigma_3' = \sigma_3 - u$ with increasing number of cycles. The increase of the amplitude of axial strain especially after the so-called "initial liquefaction" (i.e. when $u/\sigma_3 = 1$ is reached for the first time) is obvious in Figure 3b and also in the plot of the q-ε_1 hystereses in Figure 3c. After initial liquefaction several cyclic mobility loops are passed through. The corresponding butterfly-shaped effective stress path is obvious in the p-q diagrams provided for the tests with $p_0 = 100$ and 300 kPa in Figure 4. The undrained cyclic loading was stopped after completion of the cycle in which the failure criterion $|\varepsilon_1| = 10$ % was fulfilled. Similar results as those presented in Figs. 3 and 4 have been obtained by many other researchers, see e.g. [14] or [23].

Figure 5 shows the ratio of accumulated pore water pressure u^{acc} and initial effective mean pressure p_0 as a function of the number of cycles. The data measured in all 13 undrained tests is provided. A sample is liquefied at $u^{\text{acc}}/p_0 = 1$. As expected, for a certain initial effective mean stress p_0, the rate of pore water pressure accumulation $\dot{u}^{\text{acc}}$ increases considerably with increasing stress amplitude q^{ampl}. The curves of accumulated volumetric strain $\varepsilon_v^{\text{acc}}(N)$ observed in the drained cyclic tests are presented in Figure 6. For a given average mean pressure $p^{\text{av}} = p_0$, the rate of volumetric strain accumulation $\dot{\varepsilon}_v^{\text{acc}}$ also increases with increasing stress amplitude.

For each pair of drained and undrained cyclic tests the bulk modulus K was calculated from Eq. (3). The rates $\dot{u}^{\text{acc}}$ and $\dot{\varepsilon}_v^{\text{acc}}$ were obtained from the trend curves $u^{\text{acc}}(N)$ and $\varepsilon_v^{\text{acc}}(N)$ measured in the undrained or drained test, respectively. The rate of pore water pressure $\dot{u}^{\text{acc}} \approx \Delta u^{\text{acc}}/\Delta N$ was evaluated using increments of $\Delta u^{\text{acc}} = 10$ kPa. Before Eq. (3) can be applied, the rates have to be corrected considering the divergence of the effective average stresses, void ratios and strain amplitudes in the drained and the undrained cyclic test. During an undrained cyclic test with constant stress amplitude the average mean pressure decreases, i.e. the HCA model function f_p increases. Simultaneously, the strain amplitude $\varepsilon^{\text{ampl}}$ increases considerably, i.e. f_{ampl} increases. In the drained test p^{av} is constant and the strain amplitude does hardly change, but the void ratio e decreases with N, i.e. f_e decreases. In order to evaluate $\dot{u}^{\text{acc}}$ and $\dot{\varepsilon}_v^{\text{acc}}$ for exactly the same state, that means same values of strain amplitude $\varepsilon^{\text{ampl}}$, average void ratio e^{av}, average mean pressure p^{av} and cyclic preloading g^A, the rate $\dot{\varepsilon}_v^{\text{acc}}$ from the drained tests has been corrected by a factor f_c consisting of four multipliers:

$$f_c = \frac{f_{\text{ampl}}^{UD}}{f_{\text{ampl}}^{D}} \frac{f_e^{UD}}{f_e^{D}} \frac{f_p^{UD}}{f_p^{D}} \frac{\dot{f}_N^{UD}}{\dot{f}_N^{D}} \quad (6)$$

The indices $\sqcup^{UD}$ and $\sqcup^{D}$ indicate the undrained or drained

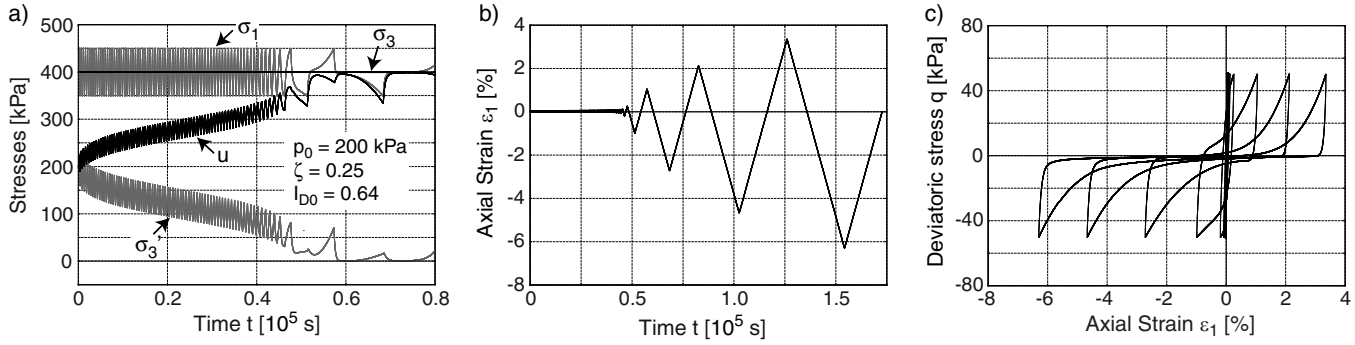

Fig. 3: *Development of a) total and effective stress components and b) axial strain with the number of cycles in a stress-controlled undrained cyclic triaxial test on medium dense fine sand. c) Deviatoric stress versus axial strain.*

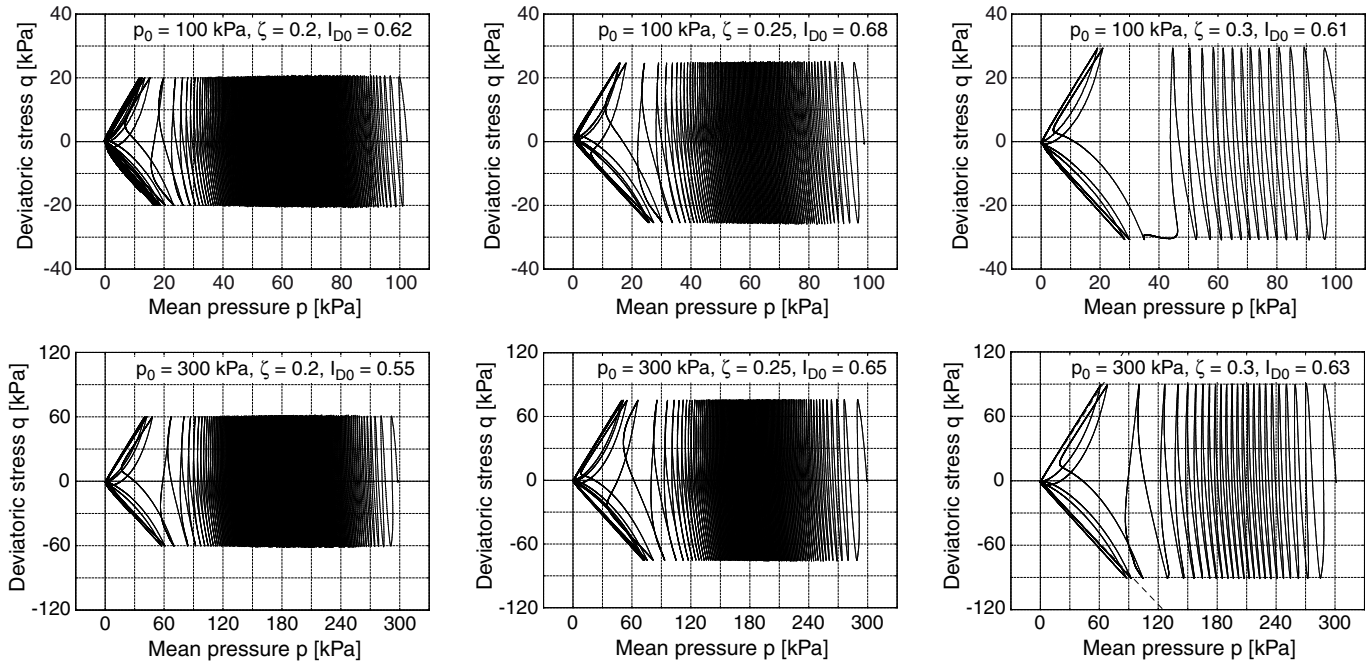

Fig. 4: *Effective stress paths in the p-q-plane measured in the undrained cyclic tests on medium dense fine sand with initial effective mean pressures p_0 = 100 or 300 kPa, respectively*

C_{ampl}	C_e	C_p	C_Y	C_{N1}	C_{N2}	C_{N3}
1.26	0.53	0.15	3.22	$1.28 \cdot 10^{-4}$	0.64	0

Table 1: HCA parameters for the fine sand determined from the drained cyclic test data

test, respectively. The functions f_{ampl}, f_e, f_p and $\dot{f}_N$ were calculated with the parameters C_{ampl}, C_e, C_p, C_Y, C_{N1}, C_{N2} and C_{N3} given in Table 1. These parameters have been determined from the data of the drained cyclic tests, following the procedure described e.g. in [19]. Note that recently the exponent C_{ampl} of the amplitude function $f_{\text{ampl}} = (\varepsilon^{\text{ampl}}/10^{-4})^{C_{\text{ampl}}}$ has been introduced as an additional material constant. A constant exponent 2.0 has been still used in [10] and [19, 20]. If one of the four multipliers in Eq. (6) was larger than 2.0 or if the strain amplitude exceeded $\varepsilon^{\text{ampl}} = 10^{-3}$ (upper border of HCA model validity) the respective data were omitted in the analysis of K.

Figure 7 shows the bulk modulus $K = \dot{u}^{\text{acc}}/\dot{\varepsilon}_v^{\text{acc}}$ determined from the 26 tests on medium dense fine sand. No

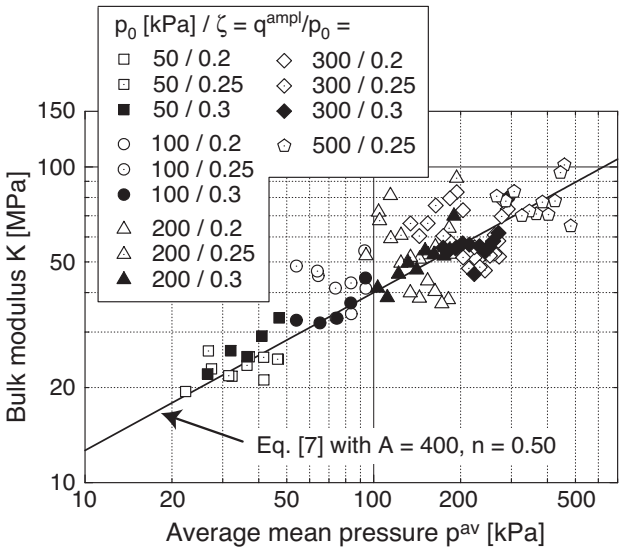

Fig. 7: *Bulk modulus $K = \dot{u}^{\text{acc}}/\dot{\varepsilon}_v^{\text{acc}}$ for medium dense fine sand as a function of average mean pressure p^{av}*

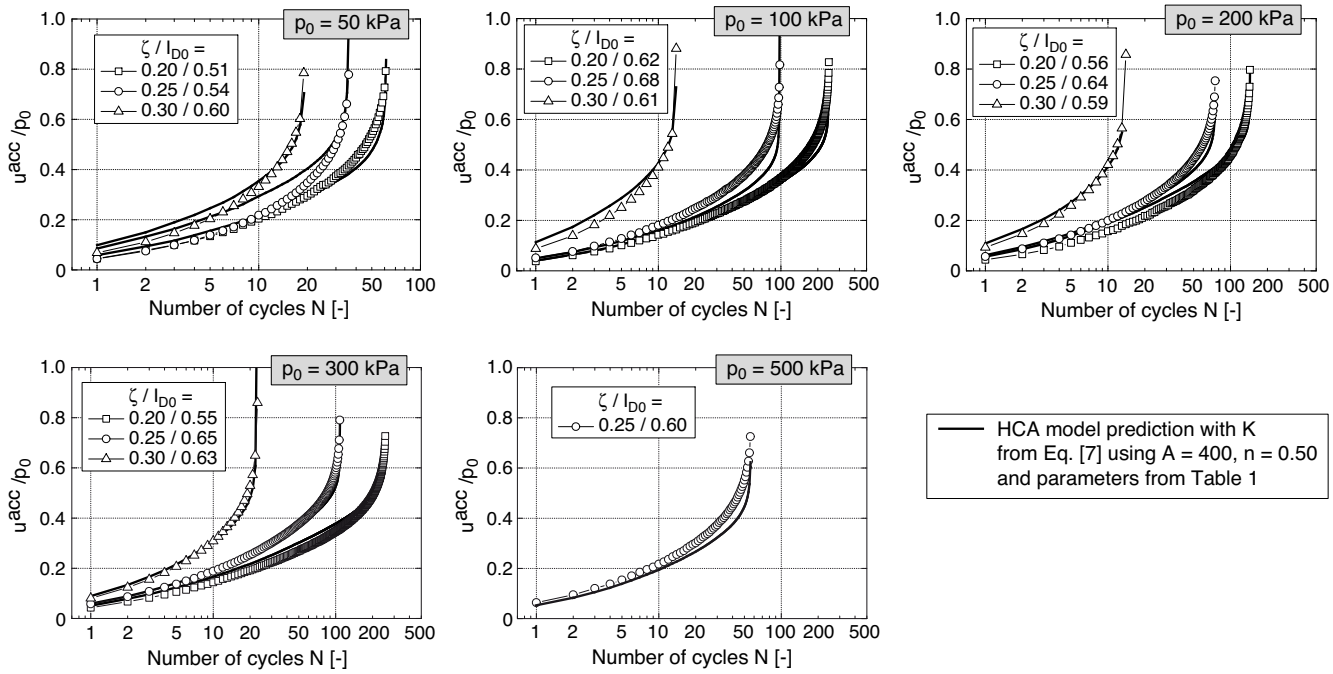

Fig. 5: *Development of normalized excess pore water pressure u^{acc}/p_0 with increasing number of cycles N in the undrained cyclic tests*

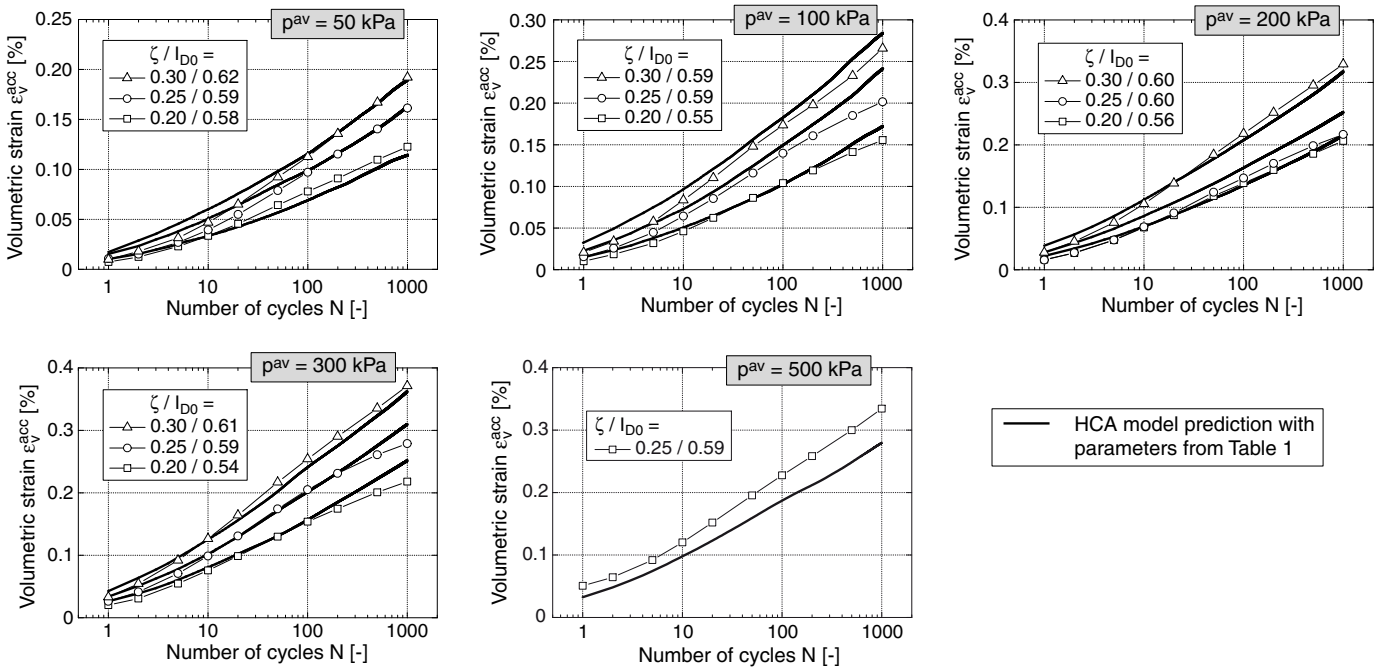

Fig. 6: *Development of residual volumetric strain ε_v^{acc} with increasing number of cycles N in the drained cyclic tests*

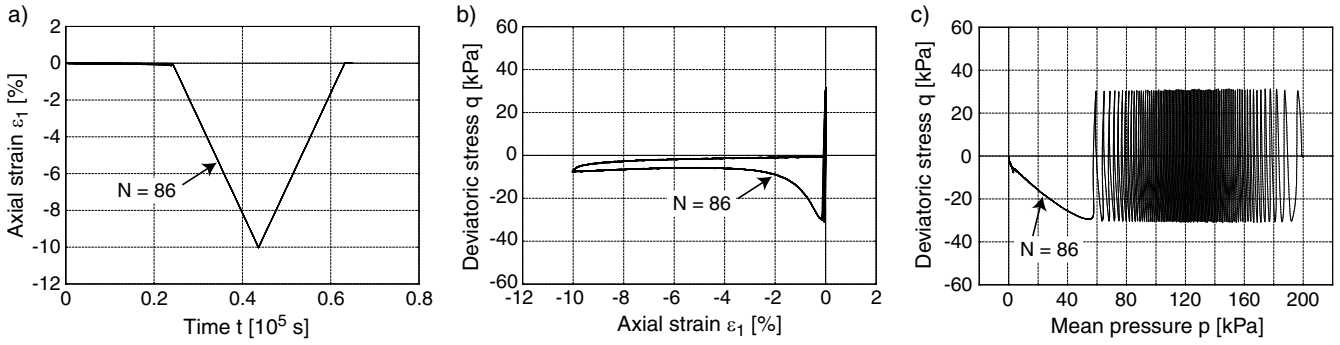

Fig. 8: *Results of an undrained cyclic test on loose fine sand (p_0 = 200 kPa, $\zeta = q^{ampl}/p_0$ = 0.15, I_{D0} = 0.26)*

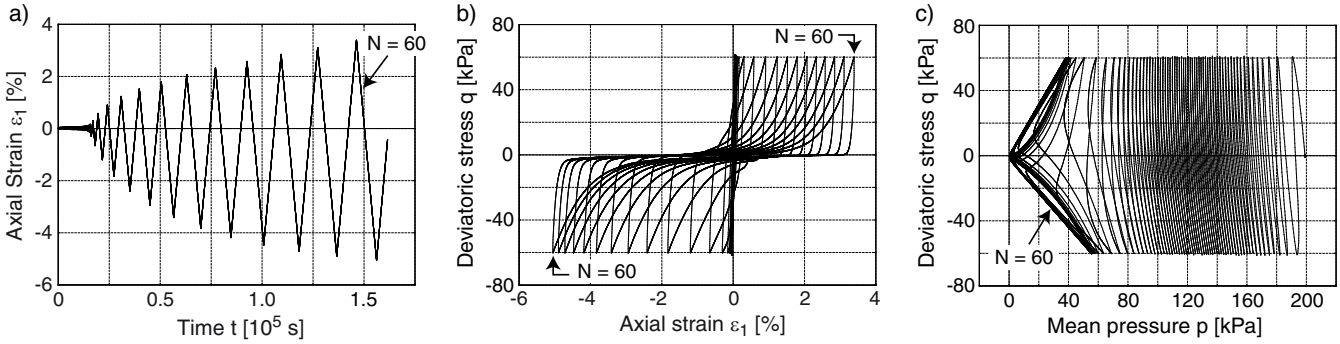

Fig. 9: *Results of an undrained cyclic test on dense fine sand (p_0 = 200 kPa, $\zeta = q^{ampl}/p_0$ = 0.30, I_{D0} = 0.80)*

significant influence of the amplitude on K could be detected from the data in Figure 7. Despite some scatter of the data, the obvious pressure-dependence of K can be approximated by

$$K = A\, p_{\mathrm{atm}}^{1-n}\, (p^{\mathrm{av}})^n \tag{7}$$

The parameters A and n of Eq. (7) can be either determined from a curve-fitting of Eq. (7) to the data in Figure 7 or from recalculations of the undrained cyclic tests with the HCA model. In these recalculations A and n are varied until the curves $u^{\mathrm{acc}}(N)$ for various pressures and amplitudes are reproduced well. Using the latter method the parameters $A = 400$ and $n = 0.50$ were found appropriate. The curves $u^{\mathrm{acc}}/p_0(N)$ from the recalculations using these parameters are given as solid curves in Fig. 5. The initial void ratios, the measured strain amplitudes $\varepsilon^{\mathrm{ampl}}(N)$ and the parameters given in Table 1 were used as input for the recalculations. Eq. (7) with $A = 400$ and $n = 0.50$ is also given as solid line in Figure 7.

The exponent $n = 0.5$ found appropriate for the HCA stiffness is in accordance with the contact of two cones according to Goddard [3]. It lies in the middle of values usually measured for a small-strain stiffness. The parameter A and thus the magnitude of K is, however, considerably smaller than in the case of a small-strain stiffness [20].

Recalculations of the drained cyclic tests with the HCA model have been added as thick solid curves in Figure 6. The HCA model prediction agrees quite well with the measured curves $\varepsilon_v^{\mathrm{acc}}(N)$. From Figures 5 and 6 it can be concluded that the HCA model with a single set of parameters (C_{ampl}, $\ldots C_{N3}$) in combination with the pressure-dependent bulk modulus according to Eq. (7) describes well both, the accumulation of pore water pressure in the undrained cyclic tests and the accumulation of volumetric strain in the drained cyclic tests.

2.2 Density-dependence of K

The density-dependence of the bulk modulus K was studied in six tests on loose (I_{D0} = 0.22 - 0.26) and six tests on dense (I_{D0} = 0.76 - 0.82) samples of the fine sand. For each density three different initial pressures p_0 = 100, 200 and 300 kPa were applied. The amplitude-pressure ratio was chosen as $\zeta = 0.15$ for the loose specimens while it was 0.30 in the tests on the dense ones. For each density three specimens were tested under drained conditions while the remaining three were tested undrained.

Figure 8 presents typical results from an undrained cyclic test on loose sand, while similar data for dense sand is given in Figure 9. For the loose samples failure was defined when an axial strain $|\varepsilon_1| = 10$ % was reached while $|\varepsilon_1| = 5$ % was chosen as the failure criterion for the dense sand. The loose sand failed due to large extensional strain developed within a single cycle. In contrast, several cyclic mobility loops with a gradual increase of the axial strain amplitude were observed for the dense sand.

The curves $u^{\mathrm{acc}}/p_0(N)$ measured in the undrained cyclic tests on the loose and dense sand samples are provided in Figure 10a and 10d while the curves $\varepsilon_v^{\mathrm{acc}}(N)$ from the drained tests are given in Figure 10b and 10e. The bulk modulus K evaluated from these curves is shown in Figure 10c and 10f. The prediction of Eq. (7) with the parameters found appropriate for the medium dense sand ($A = 400$, $n = 0.5$) has been added as dashed line in Figure 10c and 10f. Despite the significant scatter of data, the increase of K with increasing density is obvious in Figure 10c and 10f. The majority of K-data for loose sand plots below the average curve for the medium dense sand (Figure 10c), while most of the data points for dense samples lie above (Figure

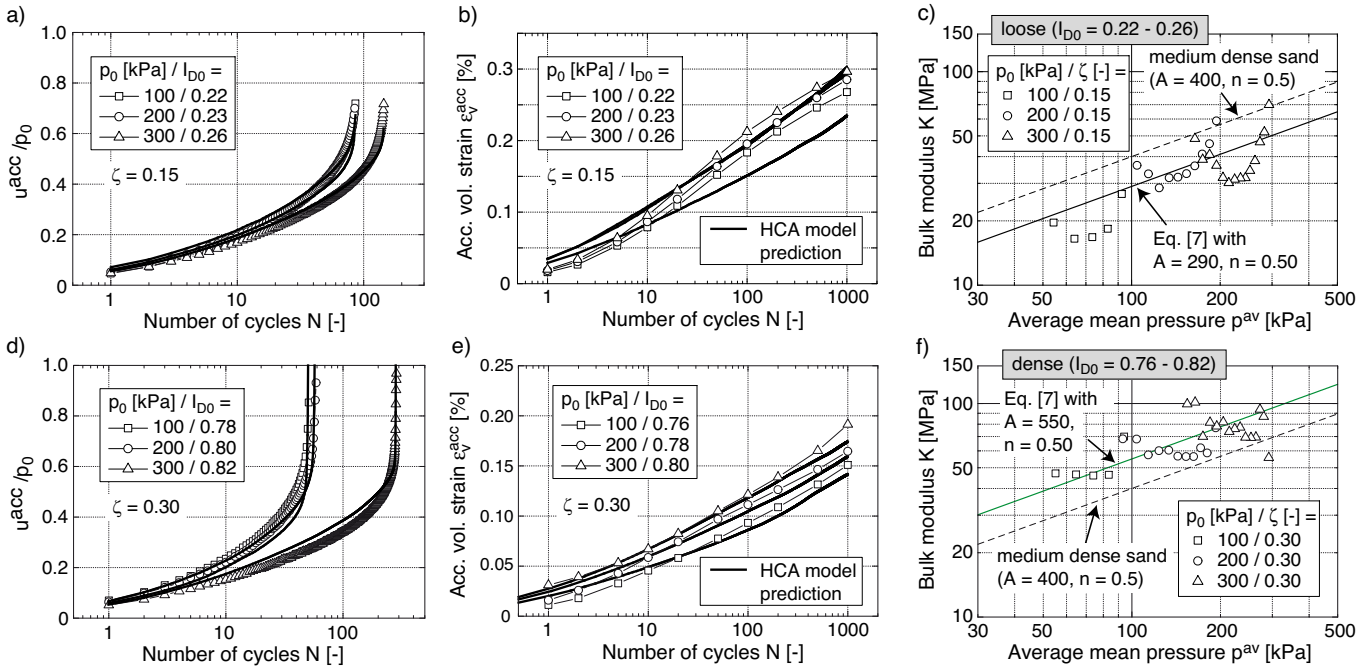

Fig. 10: *Curves $u^{acc}/p_0(N)$ and $\varepsilon_v^{acc}(N)$ measured in the undrained or drained cyclic tests and bulk modulus $K(p^{av})$ determined from the tests on a-c) loose and d-f) dense fine sand. The predictions with the HCA model have been made using Eq. (7) with either A = 290 and n = 0.5 (loose sand) or A = 550 and n = 0.5 (dense sand) and with the parameters summarized in Table 1.*

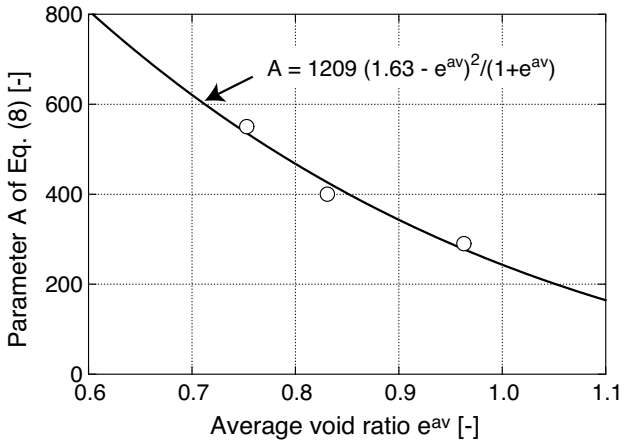

Fig. 11: *Parameter A in Eq. (7) as a function of average void ratio e^{av}*

10f).

Appropriate parameters A and n of Eq. (7) for the loose and the dense sand have been determined from recalculations of the undrained cyclic tests. The exponent n = 0.5 was found suitable for all tested densities. The curves $u^{acc}/p_0(N)$ measured for the loose sand can be reproduced well with a parameter A = 290 (see solid curves in Figure 10a), while A = 550 is appropriate for dense sand (solid curves in Figure 10d). The relationships $K(p^{av})$ established by Eq. (7) with A = 290 and n = 0.5 or with A = 550 and n = 0.5, respectively, have been added as solid lines in Figure 10c and 10f.

The volumetric strain accumulation curves $\varepsilon_v^{acc}(N)$ predicted by the HCA model with the parameters in Table 1 have been added as solid curves in Figure 10b and 10e. The good agreement with the experimental data for loose and dense sand confirms the void ratio function f_e of the HCA model.

In Figure 11 the A parameter of Eq. (7) obtained from the tests on loose, medium dense and dense sand is plotted versus an average void ratio e^{av} of the test series. The obvious decrease of A with increasing void ratio can be described by $A = 1209\ \frac{(1.63-e^{av})^2}{1+e^{av}}$. A similar void ratio function is usually applied for the small-strain shear modulus of sand [4, 21]. Therefore, the density- and pressure-dependence of the bulk modulus for fine sand can be expressed by:

$$K = 1209\ \frac{(1.63-e^{av})^2}{1+e^{av}}\ 100^{0.5}\ (p^{av})^{0.5} \qquad (8)$$

2.3 Stress ratio-dependence of K

In order to quantify the influence of the average stress ratio η^{av} on K six additional tests have been performed with a consolidation stress ratio η_0 = 0.75. The data of these tests has been compared to that for isotropically consolidated samples (η_0 = 0). The cyclic loading was commenced at three different initial pressures (p_0 = 100, 200 and 300 kPa). All samples were medium dense (I_{D0} = 0.57 - 0.66) and the amplitude-pressure ratio was chosen as ζ = 0.25 in all tests. A typical test result is provided in Figure 12. This figure shows the accumulation of residual axial strain with the number of cycles, the q-ε_1 hystereses and the effective stress path in the p-q-plane measured in the test with p_0 = 200 kPa. The excess pore water pressure tends to reach an asymptotic value after a certain number of cycles (Figure 13). The accumulation of axial strain continues even when the asymptotic effective stress has been almost reached (Figure 12a).

During an undrained cyclic test with anisotropic consolidation stresses the average stress ratio η^{av} increases due to the decrease of p^{av} while q^{av} remains constant. The increase

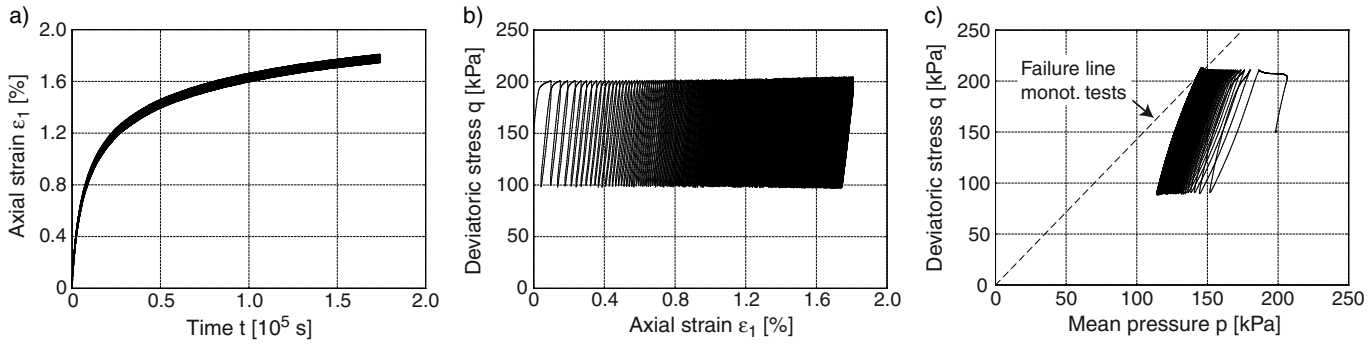

Fig. 12: *Results of an undrained cyclic test with anisotropic consolidation stress (p_0 = 200 kPa, η_0 = 0.75, I_{D0} = 0.66)*

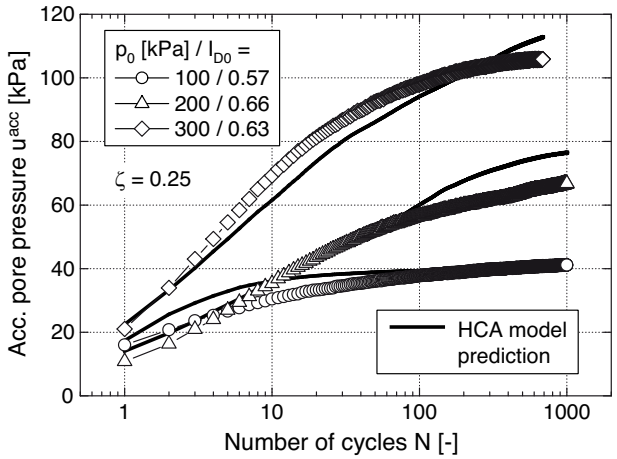

Fig. 13: *Curves of accumulated pore water pressure $u^{acc}(N)$ measured in the undrained cyclic tests on medium-dense fine sand with anisotropic consolidation stresses (η_0 = 0.75). The prediction with the HCA model is based on Eq. (7) with A = 400 and n = 0.5 and the parameters given in Table 1.*

of η^{av} implies an increase of the intensity of accumulation, i.e. a larger HCA model function f_Y. Furthermore, the direction of accumulation becomes more deviatoric with increasing η^{av}, i.e. the ratio $1/\omega = \dot{\varepsilon}_q^{acc}/\dot{\varepsilon}_v^{acc}$ gets larger. Since η^{av} is constant in the drained tests, for the evaluation of the bulk modulus K at $\eta^{av} > 0$, the correction factor f_c introduced by Eq. (6) has to be extended by two additional factors, considering f_Y and ω:

$$f_c = \ldots \cdot \frac{f_Y^{UD}}{f_Y^{D}} \; \frac{\sqrt{1/3 + 3/2(1/\omega^D)^2}}{\sqrt{1/3 + 3/2(1/\omega^{UD})^2}} \qquad (9)$$

with $\omega = (M^2 - (\eta^{av})^2)/(2\eta^{av})$ adapted from the Modified Cam-clay model. The K-values evaluated for the three pairs of drained and undrained cyclic tests consolidated at η_0 = 0.75 lie close to the data for isotropic stresses given in Figure 7. Furthermore, the pore water pressure accumulation measured in the undrained tests with η_0 = 0.75 can be well reproduced with Eq. (7) using the parameters A = 400 and n = 0.5 derived for isotropic consolidation stresses (see the solid curves in Figure 13). This comparison of the tests with η_0 = 0 and η_0 = 0.75 suggests that the stress ratio η^{av} need not be considered in the equation for bulk modulus K.

2.4 Comparison with earlier study on medium coarse sand

The relationship $K(p^{av})$ found in the present study for medium dense fine sand agrees well with that reported in [20] for medium coarse sand (d_{50} = 0.55 mm, C_u = 1.8). Eq. (7) with parameters A = 467 and n = 0.46 was found appropriate for medium dense specimens of the medium coarse sand in [20]. These parameters are close to those (A = 500 and n = 0.50) for medium dense fine sand derived in the present study. The comparison of the test results for fine and medium coarse sand suggests that bulk modulus K is similar for uniform sands having a comparable uniformity coefficient. However, the dependence of K on parameters like grain size distribution curve or grain shape needs a more detailed study in future.

3 Experimental study on Poisson's ratio ν

The dependence of Poisson's ratio ν on strain amplitude, void ratio, pressure and stress ratio was studied in several undrained cyclic tests with anisotropic consolidation and strain cycles. The first irregular cycle was applied drained in all tests, i.e. the average effective stress path during the regular cycles starts from the consolidation stress p_0, η_0.

3.1 Dependence of ν on amplitude

First, three tests with different strain amplitudes $\varepsilon_1^{ampl} = 4 \times 10^{-4}$, 6×10^{-4} or 8×10^{-4} have been performed on medium dense specimens consolidated at p_0 = 200 kPa and η_0 = 0.75. The effective stress paths measured in these tests are given in the p-q plane in Figure 14. Independently of the strain amplitude a zero effective stress state (i.e. the origin of the p-q-plane) was reached after a certain number of cycles. The average effective stress paths (measured at $\varepsilon_1 = 0$) from these three tests have been summarized in the p^{av}-q^{av} diagram given in Figure 15a. No influence of the strain amplitude on the stress relaxation paths - and thus on ν - could be detected in the range of tested strain amplitudes.

3.2 Dependence of ν on density

The void ratio-dependence of ν has been studied in five tests with different initial relative densities lying in the range $0.38 \le I_{D0} \le 0.97$. The initial stress (p_0 = 200 kPa, η_0 = 0.75) and the strain amplitude ($\varepsilon_1^{ampl} = 6 \times 10^{-4}$) were the same in all tests. The effective stress paths measured in three of these tests are given in Figure 16. The p^{av}-q^{av} stress paths for the five different densities almost

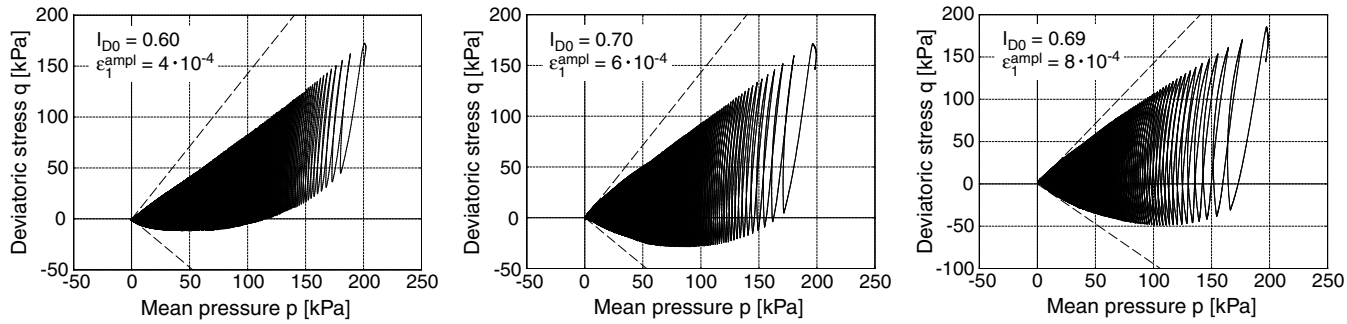

Fig. 14: *Effective stress paths in the p-q-plane in undrained cyclic tests with anisotropic consolidation stresses and strain cycles applied with different amplitudes* $\varepsilon_1^{ampl} = 4$, *6 or* 8×10^{-4} *(all tests:* $p_0 = 200$ *kPa,* $\eta_0 = 0.75$*)*

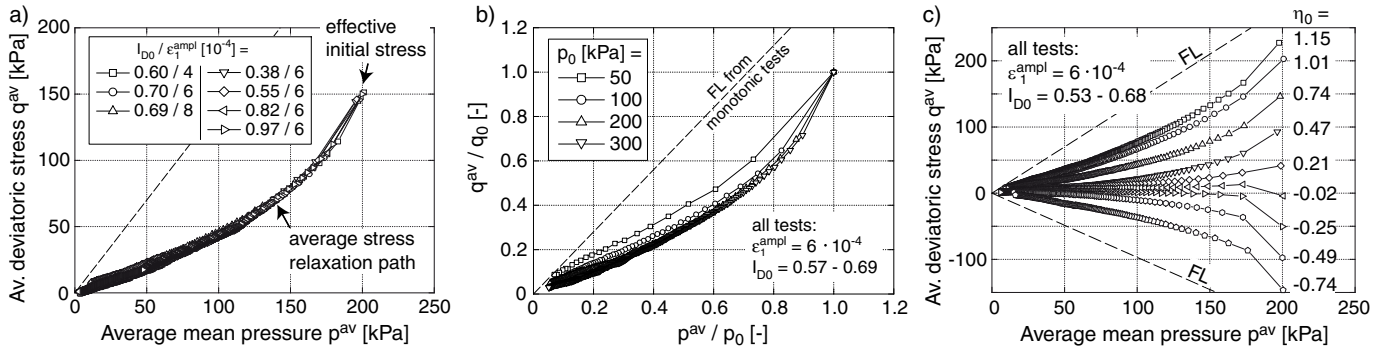

Fig. 15: *Paths of the average effective stress in undrained tests with strain cycles and different a) strain amplitudes and initial relative densities, b) effective initial pressures* p_0 *and c) initial stress ratios* $\eta_0 = q_0/p_0$

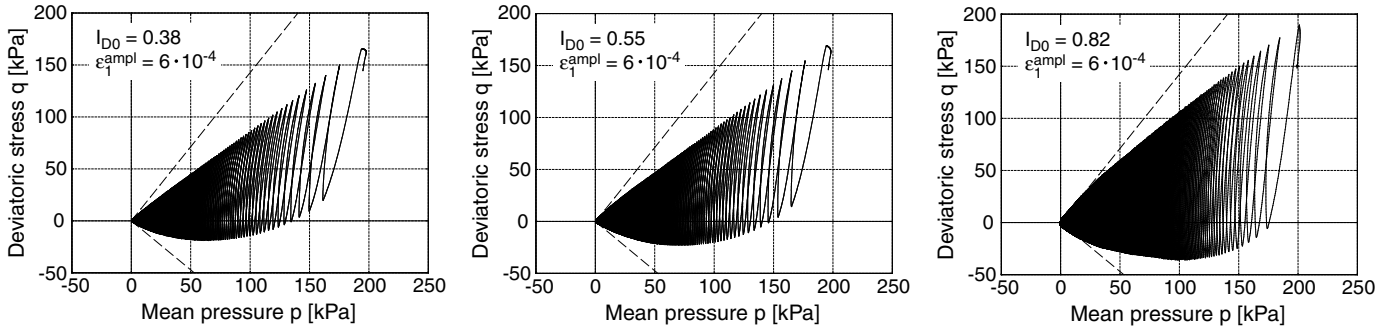

Fig. 16: *Effective stress paths in the p-q-plane in undrained tests with anisotropic consolidation stresses and strain cycles applied on samples with different initial relative densities* $I_{D0} = 0.38$, *0.55 and 0.82 (all tests:* $\varepsilon_1^{ampl} = 6 \times 10^{-4}$, $p_0 = 200$ *kPa,* $\eta_0 = 0.75$*)*

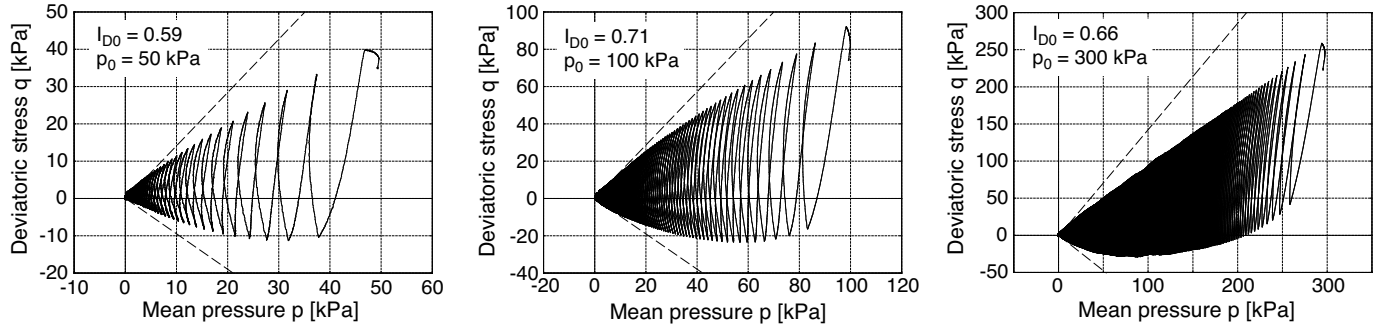

Fig. 17: *Effective stress paths in the p-q-plane in undrained tests with anisotropic consolidation stresses and strain cycles commenced at different initial effective mean pressures* p_0 *(all tests:* $\varepsilon_1^{ampl} = 6 \times 10^{-4}$, $\eta_0 = 0.75$*)*

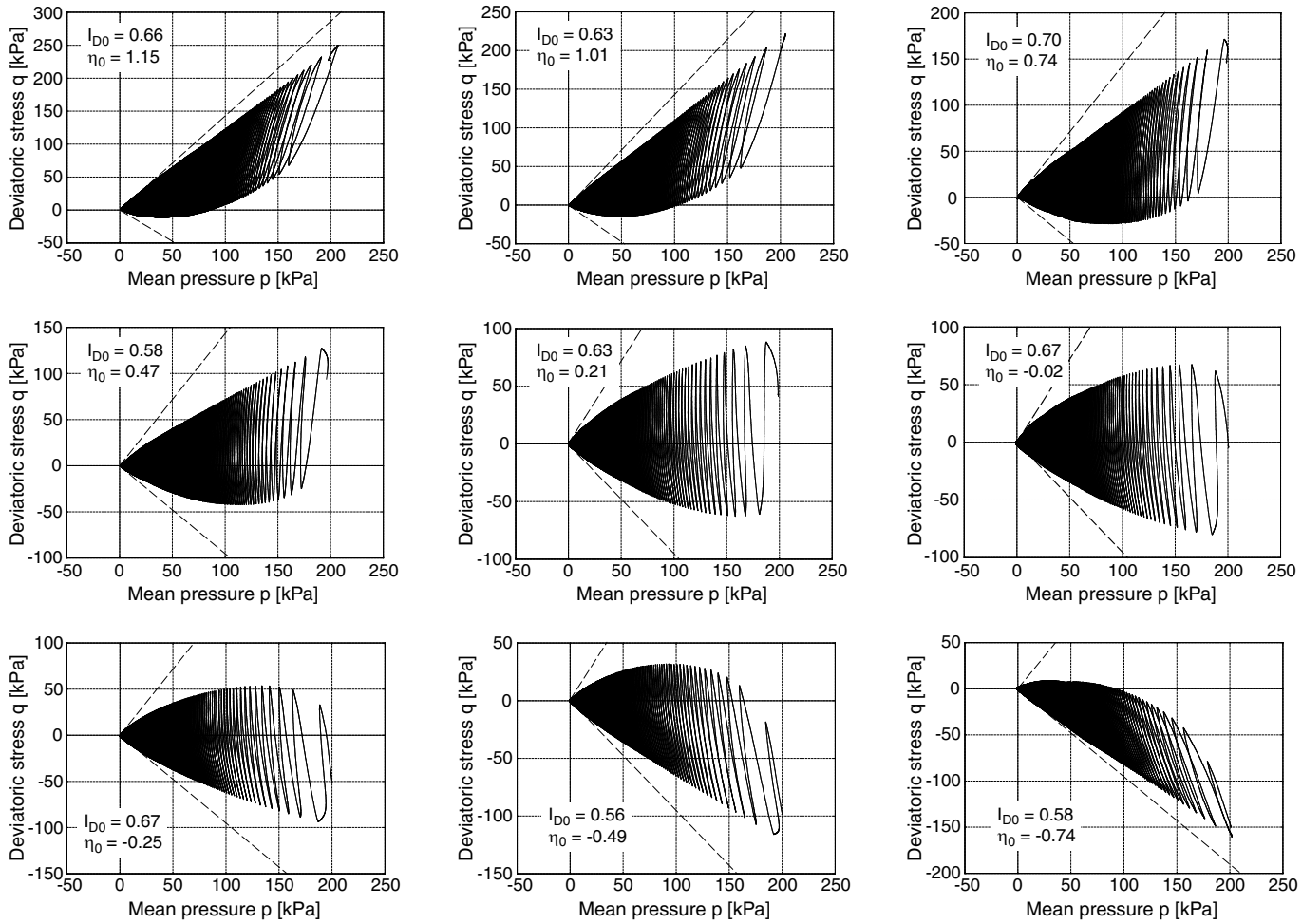

Fig. 18: Effective stress paths in the p-q-plane in undrained tests with strain cycles with different initial stress ratios η_0 (all tests: $\varepsilon_1^{\mathrm{ampl}} = 6 \times 10^{-4}$, $p_0 = 200$ kPa)

coincide (Figure 15a). Therefore, it can be concluded that ν is density-independent.

3.3 Dependence of ν on pressure

The pressure-dependence of ν has been inspected in four tests with different initial mean pressures p_0 between 50 and 300 kPa. All samples were medium dense, consolidated at $\eta_0 = 0.75$ and subjected to strain cycles with an amplitude $\varepsilon_1^{\mathrm{ampl}} = 6 \times 10^{-4}$. The effective stress paths measured in the tests with $p_0 = 50$, 100 and 300 kPa are given in Figure 17. When the average effective stress paths from the tests with different initial pressures are plotted in a diagram with normalized axes (p^{av}/p_0 and q^{av}/q_0, Figure 15b), apart from some deviation for $p_0 = 50$ kPa, the shape of the stress relaxation curves nearly coincides. Therefore, for practical purposes ν can be treated pressure-independent.

3.4 Dependence of ν on stress ratio

Finally, the influence of the initial stress ratio η_0 has been tested on medium dense specimens. Stress ratios between -0.75 and 1.15 have been tested. All tests were started at $p_0 = 200$ kPa and performed with the same strain amplitude $\varepsilon_1^{\mathrm{ampl}} = 6 \times 10^{-4}$. The effective stress paths measured in these tests are collected in Figure 18. Independently of the initial stress ratio a zero effective stress has been reached in all tests after a certain number of cycles. This is also obvious from the average stress paths shown in Figure 15c.

In two additional tests with $\eta_0 = -0.50$ and 0.75 the first irregular cycle was applied undrained (and not drained as in all other tests). However, nearly the same shape of the average effective stress path as in the tests with a drained first cycle was obtained.

In order to quantify Poisson's ratio ν, the strain-controlled undrained cyclic tests were recalculated with the HCA model. Several calculations with different ν-values were performed for a test until the measured average effective stress path could be reproduced satisfactorily. Figure 19 compares some of the measured p^{av}-q^{av}-curves with the predictions made by the HCA model (thick solid curves) using the optimum ν-values given in the gray-shaded boxes. For initial stress ratios in the range $0 \leq \eta_0 \leq 0.75$, a Poisson's ratio $\nu \approx 0.3$ is appropriate - independently of strain amplitude, soil density and initial pressure p_0 (Figure 19c-f). For initial stress ratios $\eta_0 > 0.75$ larger Poisson's ratios are necessary (e.g. $\nu = 0.36$ for $\eta_0 = 1.01$ and $\nu = 0.39$ for $\eta_0 = 1.15$, Figure 19a,b). The same conclusion can be drawn for $|\eta_0|$-values in the triaxial extension regime ($\nu = 0.34$ for $\eta_0 = -0.74$, Figure 19h). The large increase of the deviatoric stress q^{av} during the first regular cycle measured in the tests with $\eta_0 = -0.25$ and -0.49 can be reproduced

only with very low ν-values (e.g. $\nu = 0.10$ for η_0 = -0.49, Figure 19g).

The stress-ratio dependence of Poisson's ratio could be described e.g. by the formula $\nu = 0.29+0.12(\eta_0/M)^2$. However, a constant mean value $\nu = 0.32$ may be sufficient for a practical application of the HCA model. Except the initial stress ratios η_0 = 1.15, -0.25 and -0.49, the p^{av}-q^{av}-curves measured in all tests can be sufficiently well reproduced with $\nu = 0.32$ (see the thick dashed curves given in Figure 19). Therefore, the choice of $\nu = 0.32$ is recommended for calculations with the HCA model. The Poisson's ratio $\nu = 0.32$ found appropriate for the HCA stiffness lies in the middle of values usually measured for a small-strain stiffness [22].

Figure 20 shows a comparison between the curves of accumulated pore water pressure $u^{\mathrm{acc}}(N)$ measured in four of the strain-controlled tests and predictions made by the HCA model, using the parameters in Table 1, bulk modulus according to Eq. (8) and $\nu = 0.32$. A good congruence between the experimental and the predicted $u^{\mathrm{acc}}(N)$-data can be stated for the initial phase of the tests, i.e. until a pore pressure ratio $u^{\mathrm{acc}}/p_0 \approx 0.8$ is reached. During the strain cycles applied at $u^{\mathrm{acc}}/p_0 > 0.8$, the pore pressure accumulation measured in the tests is larger than that predicted by the HCA model.

There are several possible causes for this underestimation of the accumulation rate at low effective stresses $p^{\mathrm{av}} <$ 50 kPa: First, the HCA model functions f_p or f_{ampl} could be underestimated at low p-values since they have been calibrated based on drained cyclic tests with $p^{\mathrm{av}} \geq 50$ kPa. Drained cyclic tests with lower pressures are, however, difficult to perform in the laboratory. Second, the bulk modulus K may be underestimated at low pressures. The data in Figure 7 suggests, however, that at least in the range 20 kPa $\leq p^{\mathrm{av}} \leq$ 50 kPa, K is adequately described by Eq. (8). Third, several authors (e.g. [13], [23] and [11]) observed a latent accumulation of strain occurring due to cycles applied in the liquefied state, i.e. at $\boldsymbol{\sigma}^{\mathrm{av}} = \mathbf{0}$. It becomes visible as volumetric strain during reconsolidation. As an example, the results of an experiment performed by Niemunis et al. [11] are given in Figure 21. The medium dense sample of a silty fine sand was liquefied three times by strain cycles ($\varepsilon^{\mathrm{ampl}} = 2 \times 10^{-3}$). After a certain number of cycles applied in the liquefied state the drainage was opened to allow for reconsolidation. The magnitude of volumetric strain during reconsolidation increased with increasing number of strain cycles applied at $\boldsymbol{\sigma}^{\mathrm{av}} = \mathbf{0}$. This latent accumulation at $\boldsymbol{\sigma}^{\mathrm{av}} = \mathbf{0}$ has not been implemented into the HCA model so far. The larger accumulation rates near liquefaction in the experiments presented in Figure 20 may be connected with this phenomenon. The cumulative behaviour of sand in the (nearly) liquefied state is not well understood yet and thus needs further experimental studies. Such deficit does not become evident in the recalculations of the stress-controlled experiments (e.g. Figure 5) where $u^{\mathrm{acc}}/p_0 \approx 0.8$ is immediately followed by full liquefaction and large strain amplitudes. The large values of $\varepsilon^{\mathrm{ampl}}$ lead to large accumulation rates $\dot{u}^{\mathrm{acc}}$ predicted by the HCA model via f_{ampl}.

4 Summary, conclusions and outlook

The "elastic stiffness" E used in the constitutive equation $\dot{\boldsymbol{\sigma}}^{\mathrm{av}} = \mathsf{E} : (\dot{\boldsymbol{\varepsilon}}^{\mathrm{av}} - \dot{\boldsymbol{\varepsilon}}^{\mathrm{acc}} - \dot{\boldsymbol{\varepsilon}}^{\mathrm{pl}})$ of the high-cycle accumulation (HCA) model [10] has been further inspected based on drained and undrained cyclic tests with strain or stress control performed on a fine sand.

Bulk modulus $K = \dot{u}^{\mathrm{acc}}/\dot{\varepsilon}_v^{\mathrm{acc}}$ has been evaluated from pairs of drained and undrained cyclic triaxial tests with similar initial state and stress amplitudes. The rate $\dot{u}^{\mathrm{acc}}$ of pore water pressure accumulation was obtained from the undrained test while the rate of volumetric strain accumulation $\dot{\varepsilon}_v^{\mathrm{acc}}$ was gathered from the drained test. Such pairs of tests were performed with different initial densities, consolidation stresses (isotropic and anisotropic) and stress amplitudes. The pressure-dependence of bulk modulus K for medium dense fine sand was found of similar magnitude as in an earlier study on medium coarse sand [20], where membrane penetration effects may have affected the results. Due to the fine grains these effects are minimized in the present study. The new tests demonstrate, that the bulk modulus strongly decreases with increasing void ratio, but that it is rather independent of amplitude and average stress ratio $\eta^{\mathrm{av}} = q^{\mathrm{av}}/p^{\mathrm{av}}$. With the pressure- and density-dependent bulk modulus defined by Eq. (8) the HCA model can reproduce both, the accumulation of pore water pressure in the undrained cyclic tests and the accumulation of volumetric strain in the drained cyclic tests.

Poisson's ratio ν was quantified from the shape of the stress relaxation path measured in undrained triaxial tests with anisotropic consolidation and strain cycles. It has been demonstrated that ν is almost independent of amplitude, density and pressure. Although higher values of ν would more accurately describe the measured p^{av}-q^{av}-curves in the tests with high initial stress ratios ($\eta_0 > 1$) and significantly lower values would be appropriate for an initial stress in some parts of the triaxial extension regime ($-0.50 < \eta_0 \leq 0$), a constant value of $\nu = 0.32$ is proposed for a practical application of the HCA model, since most stress relaxation paths can be sufficiently well reproduced with this value. The pore pressure accumulation in the strain-controlled tests is well predicted by the HCA model up to $u^{\mathrm{acc}}/p_0 \approx 0.8$. Reasons for an underestimation of the accumulation rate near the liquefied state (i.e. at $u^{\mathrm{acc}}/p_0 > 0.8$) are discussed in the paper.

In future, in order to develop a simplified calibration procedure based on index properties, K and ν will be quantified for a couple of sands having different grain size distribution curves, grain shapes, etc. A simplified estimation of K based on the unloading curve in an oedometric compression test as suggested in [20] will be also further investigated.

The number of cycles applied in the experiments of this paper is usually less than 1,000, mainly due to liquefaction in the undrained tests. Some experiments even had less than 100 cycles. Such relatively low number of cycles could be eventually treated by a conventional constitutive model formulated with stress and strain rates. Calculations with the hypoplastic model extended by the intergranular strain concept [9, 15] performed by the authors showed several difficulties to reproduce the test results. For the drained tests, an accumulation $\varepsilon^{\mathrm{acc}} \sim N$ is predicted by hypoplasticity while $\varepsilon^{\mathrm{acc}} \sim \ln(N)$ is observed in the experiments. In the undrained tests a liquefied state ($\boldsymbol{\sigma}^{\mathrm{av}} = \mathbf{0}$) is reached after a sufficiently large number of cycles, independently of soil density, amplitude, initial stress and test control (with the exception of the stress-controlled tests with anisotropic consolidation stresses). The recalculations with the hypoplastic model sometimes end up in an attractor state with $\boldsymbol{\sigma}^{\mathrm{av}} \gg \mathbf{0}$. Furthermore, the dependence of the accumulation rate on density, strain amplitude and aver-

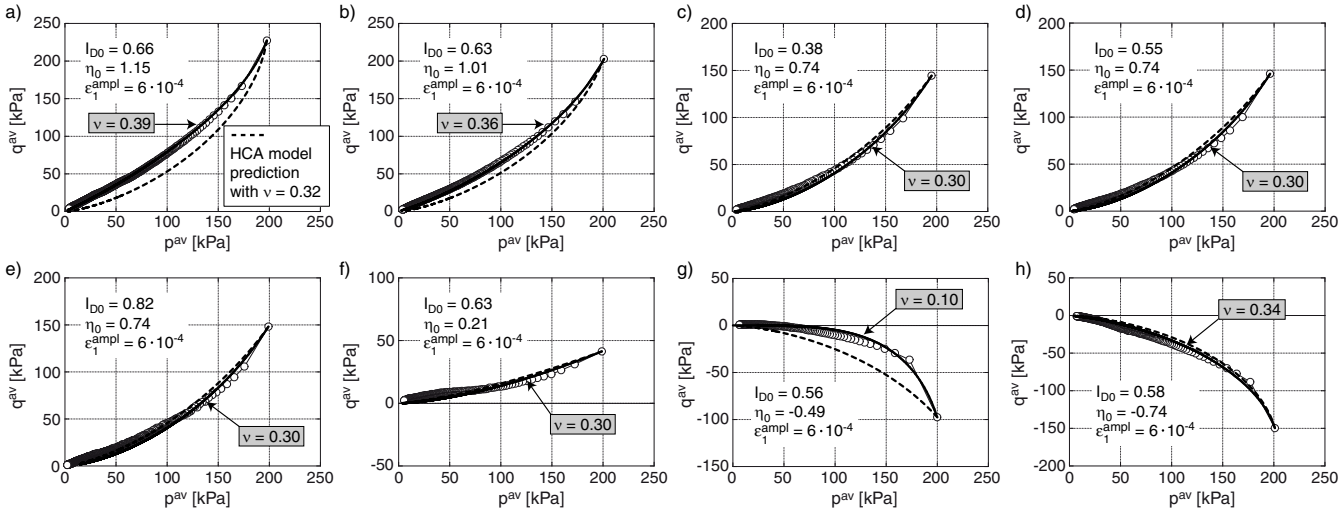

Fig. 19: *Comparison between the average effective stress paths measured in the strain-controlled undrained cyclic tests and predictions by the HCA model, using either $\nu = 0.32$ (dashed curves) or the ν-values given in the gray-shaded boxes (solid curves).*

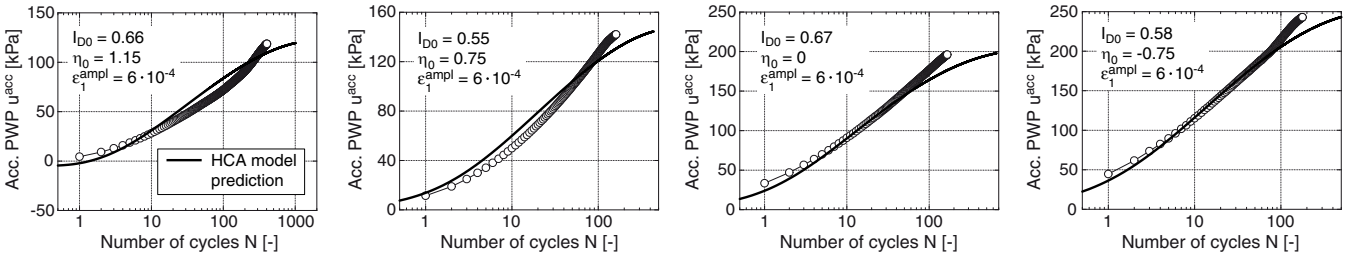

Fig. 20: *Comparison between the pore water pressure accumulation curves measured in the strain-controlled undrained cyclic tests and predictions by the HCA model, using the parameters in Table 1, bulk modulus according to Eq. (8) and $\nu = 0.32$*

age stress observed in the drained or undrained cyclic tests can be hardly reproduced by the hypoplastic model, using a single set of parameters that has been mainly calibrated from tests with monotonic loading. There are elastoplastic models that may be more suitable for cyclic loading (see e.g. [23]). However, using a HCA model even for low number of cycles ($N < 1000$) seems reasonable as well. A more detailed comparison of the experimental results with the prediction by conventional constitutive models will be presented in another paper in future.

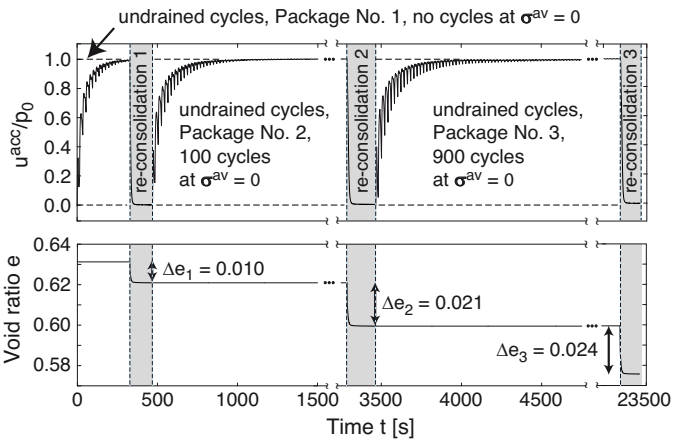

Fig. 21: *Development of pore pressure ratio u^{acc}/p_0 and void ratio in an experiment with three undrained cyclic phases each followed by a reconsolidation*

Acknowledgement

Parts of the presented study have been performed within the framework of the project "Geotechnical robustness and self-healing of foundations of offshore wind power plants" funded by the German Federal Ministry for the Environment, Nature Conservation and Nuclear Savety (BMU, project No. 0327618). Other parts were conducted within the framework of the project "Improvement of an accumulation model for high-cyclic loading" funded by German Research Council (DFG, project No. TR218/18-1). The authors are grateful to BMU and DFG for the financial support. All tests have been performed by the technician H. Borowski in the IBF soil mechanics laboratory.

References

[1] M. Abdelkrim, P. De Buhan, and G. Bonnet. A general method for calculating the traffic load-induced residual settlement of a platform, based on a structural analysis approach. *Soils and Foundations*, 46(4):401–414, 2006.

[2] G. Bouckovalas, R.V. Whitman, and W.A. Marr. Permanent displacement of sand with cyclic loading. *Journal of Geotechnical Engineering, ASCE*, 110(11):1606–1623, 1984.

[3] J.D. Goddard. Nonlinear elasticity and pressure-dependent wave speeds in granular media. *Proceedings of the Royal Society London*, 430:105–131, 1990.

[4] B.O. Hardin and F.E. Richart Jr. Elastic wave velocities in granular soils. *Journal of the Soil Mechanics and Foundations Division, ASCE*, 89(SM1):33–65, 1963.

[5] H. Hertz. Über die Berührung fester elastischer Körper. *Journal reine und angewandte Mathematik*, 92:156–171, 1881.

[6] C. Karg, S. Francois, W. Haegeman, and G. Degrande. Elasto-plastic long-term behavior of granular soils: modeling and experimental validation. *Soil Dynamics and Earthquake Engineering*, 30(8):635–646, 2010.

[7] A.E.H. Love. *A Treatise on the Mathematical Theory of Elasticity*. Cambridge University Press, 1892.

[8] W.A. Marr and J.T. Christian. Permanent displacements due to cyclic wave loading. *Journal of the Geotechnical Engineering Division, ASCE*, 107(GT8):1129–1149, 1981.

[9] A. Niemunis and I. Herle. Hypoplastic model for cohesionless soils with elastic strain range. *Mechanics of Cohesive-Frictional Materials*, 2:279–299, 1997.

[10] A. Niemunis, T. Wichtmann, and T. Triantafyllidis. A high-cycle accumulation model for sand. *Computers and Geotechnics*, 32(4):245–263, 2005.

[11] A. Niemunis, T. Wichtmann, and Th. Triantafyllidis. Long-term deformations in soils due to cyclic loading. In W. Wu and H.S. Yu, editors, *Springer Proceedings in Physics*, volume 106, pages 427–462. Springer, 2005.

[12] A. Sawicki and W. Świdziński. Mechanics of a sandy subsoil subjected to cyclic loadings. *Int. J. Numer. Anal. Meth. Geomech.*, 13:511–529, 1989.

[13] Y. Shamoto, M. Sato, and J.-M. Zhang. Simplified estimation of earthquake-induced settlements in saturated sand deposits. *Soils and Foundations*, 36(1):39–50, 1996.

[14] I. Towhata. *Geotechnical Earthquake Engineering*. Springer, 2008.

[15] P.-A. von Wolffersdorff. A hypoplastic relation for granular materials with a predefined limit state surface. *Mechanics of Cohesive-Frictional Materials*, 1:251–271, 1996.

[16] T. Wichtmann. Explicit accumulation model for non-cohesive soils under cyclic loading. PhD thesis, Publications of the Institute of Soil Mechanics and Foundation Engineering, Ruhr-University Bochum, Issue No. 38.

[17] T. Wichtmann, A. Niemunis, and T. Triantafyllidis. Strain accumulation in sand due to cyclic loading: drained triaxial tests. *Soil Dynamics and Earthquake Engineering*, 25(12):967–979, 2005.

[18] T. Wichtmann, A. Niemunis, and T. Triantafyllidis. Strain accumulation in sand due to cyclic loading: drained cyclic tests with triaxial extension. *Soil Dynamics and Earthquake Engineering*, 27(1):42–48, 2007.

[19] T. Wichtmann, A. Niemunis, and T. Triantafyllidis. Validation and calibration of a high-cycle accumulation model based on cyclic triaxial tests on eight sands. *Soils and Foundations*, 49(5):711–728, 2009.

[20] T. Wichtmann, A. Niemunis, and T. Triantafyllidis. On the "elastic" stiffness in a high-cycle accumulation model for sand: a comparison of drained and undrained cyclic triaxial tests. *Canadian Geotechnical Journal*, 47(7):791–805, 2010.

[21] T. Wichtmann and T. Triantafyllidis. On the influence of the grain size distribution curve of quartz sand on the small strain shear modulus $G_{\max}$. *Journal of Geotechnical and Geoenvironmental Engineering, ASCE*, 135(10):1404–1418, 2009.

[22] T. Wichtmann and T. Triantafyllidis. On the influence of the grain size distribution curve on P-wave velocity, constrained elastic modulus $M_{\max}$ and Poisson's ratio of quartz sands. *Soil Dynamics and Earthquake Engineering*, 30(8):757–766, 2010.

[23] J.-M. Zhang and G. Wang. Large post-liquefaction deformation of sand, part I: physical mechanism, constitutive description and numerical algorithm. *Acta Geotechnica*, 7:69–113, 2012.

List of symbols

B	Skempton's B-value
e	Void ratio
e^{av}	Average void ratio
ε_1	Axial strain
ε_3	Lateral strain
ε_v	Volumetric strain ($= \varepsilon_1 + 2\varepsilon_3$ for triaxial tests)
ε_q	Deviatoric strain ($= 2/3(\varepsilon_1 - \varepsilon_3)$ for triaxial tests)
$\varepsilon^{\mathrm{ampl}}$	Strain amplitude
$\varepsilon^{\mathrm{acc}}$	Residual (accumulated) strain
$\dot{\varepsilon}^{\mathrm{acc}}$	Intensity of strain accumulation
$\dot{\varepsilon}_v^{\mathrm{acc}}$	Rate of volumetric strain accumulation
$\boldsymbol{\varepsilon}^{\mathrm{av}}$	Average strain tensor
$\dot{\boldsymbol{\varepsilon}}^{\mathrm{av}}$	Trend of average strain
$\dot{\boldsymbol{\varepsilon}}^{\mathrm{acc}}$	Rate of strain accumulation
$\dot{\boldsymbol{\varepsilon}}^{\mathrm{pl}}$	Plastic strain rate
E	Young's modulus
E	"Elastic" stiffness of HCA model
φ_c	Critical friction angle
f_{ampl}	Amplitude function (HCA model)
f_c	Correction factor
f_e	Void ratio function (HCA model)
f_N	Function for cyclic preloading (HCA model)
f_p	Pressure function (HCA model)
f_Y	Stress ratio function (HCA model)
f_π	Function for polarization changes (HCA model)
g^A	Historiotropic variable (HCA model)
G	Shear modulus
η	Stress ratio
η^{av}	Average stress ratio
I_D	Relative density
K	Bulk modulus
M	Critical stress ratio
$\mathbf{m}$	Direction of strain accumulation
ν	Poisson's ratio
N	Number of cycles
p	Effective mean pressure ($= (\sigma'_1 + 2\sigma'_3)/3$ in triaxial tests)
p^{av}	Average effective mean pressure
$\boldsymbol{\pi}$	Historiotropic variable (HCA model)
q	Deviatoric stress ($= \sigma_1 - \sigma_3$ in triaxial tests)
q^{ampl}	Deviatoric stress amplitude
σ_1	Total axial stress
σ'_1	Effective axial stress
σ_3	Total lateral stress
σ'_3	Effective lateral stress
$\boldsymbol{\sigma}$	Effective stress tensor
$\boldsymbol{\sigma}^{\mathrm{av}}$	Average effective stress tensor
$\dot{\boldsymbol{\sigma}}^{\mathrm{av}}$	Trend of average effective stress
u	Pore water pressure
u^{acc}	Accumulated pore water pressure
$\dot{u}^{\mathrm{acc}}$	Rate of pore water pressure accumulation
ζ	Amplitude-pressure ratio ($= q^{\mathrm{ampl}}/p_0$ or $q^{\mathrm{ampl}}/p^{\mathrm{av}}$)
$\mathbf{1}$	Second-order identity tensor
I	Fourth-order identity tensor